Journal of Nanostructure in Chemistry
https://doi.org/10.1007/s40097-022-00482-5

ORIGINAL RESEARCH

Combining 2D organic and 1D inorganic nanoblocks to develop free-standing hybrid nanomembranes for conformable biosensors

Jose García-Torres[1,2,3] · Carmen Lázaro[4] · Dioulde Sylla[5] · Sonia Lanzalaco[2,4] · Maria-Pau Ginebra[1,2,6] · Carlos Alemán[2,4,6]

Received: 6 September 2021 / Accepted: 16 February 2022

Abstract

We report a simple approach to fabricate free-standing perforated 2D nanomembranes hosting well-ordered 1D metallic nanostructures to obtain hybrid materials with nanostructured surfaces for flexible electronics. Nanomembranes are formed by alternatively depositing perforated poly(lactic acid) (PLA) and poly(3,4-ethylenedioxythiophene) layers. Copper metallic nanowires (NWs) were incorporated into the nanoperforations of the top PLA layer by electrodeposition and further coated with silver via a transmetallation reaction. The combination of 2D polymeric nanomembranes and aligned 1D metallic NWs allows merging the flexibility and conformability of the ultrathin soft polymeric nanomembranes with the good electrical properties of metals for biointegrated electronic devices. Thus, we were able to tailor the nanomembrane surface chemistry as it was corroborated by SEM, EDX, XPS, CV, EIS and contact angle. The obtained hybrid nanomembranes were flexible and conformable showing sensing capacity towards H_2O_2 with good linear concentration range (0.35–10 mM), sensitivity (120 μA cm^{-2} mM^{-1}) and limit of detection (7 μm). Moreover, the membranes showed good stability, reproducibility and selectivity towards H_2O_2.

Keywords Perforated nanomembranes · Metallic nanowires · Free-standing films · Biointegrated sensors

Introduction

Flexible electronics have been extensively researched during the last decade over conventional rigid electronics due to their capacity to be integrated onto complex, curved or time dynamic surfaces like biological tissues and organs [1, 2]. Flexible electronic devices have been possible following two different approaches either through the mechanical design of conventional electronic materials (e.g., silicon, gold) making them flexible through microfabrication technologies) or the synthesis of inherently flexible and/or stretchable materials with electrical conductivity (e.g., conductive polymer-based composites) [3–6]. However, the mechanical mismatch between conventional electronic materials (generally with Young's moduli > 10^{10} Pa) and the biological tissues (generally with Young's moduli < 10^6 Pa) or the low electrical properties of the polymer-based composites with embedded electrically conductive fillers are key hurdles in the quest for biointegrated electronic devices [7, 8].

The use of nanomaterials (NMs) in bioelectronics is very promising and revolutionary since their new or enhanced physicochemical properties compared to the bulk materials

✉ Jose García-Torres
jose.manuel.garcia-torres@upc.edu

✉ Carlos Alemán
carlos.aleman@upc.edu

1 Biomaterials, Biomechanics and Tissue Engineering Group, Department of Materials Science and Engineering and Research Center for Biomedical Engineering, Universitat Politècnica de Catalunya (UPC), 08019 Barcelona, Spain

2 Barcelona Research Center in Multiscale Science and Engineering, Universitat Politècnica de Catalunya, 08019 Barcelona, Spain

3 Institut de Recerca Sant Joan de Déu, 08034 Barcelona, Spain

4 Departament d'Enginyeria Química, EEBE, Universitat Politècnica de Catalunya, C/Eduard Maristany, 10-14, 08019 Barcelona, Spain

5 IREC-Catalonia Institute for Energy Research, 08930 Sant Adrià de Besòs, Spain

6 Institute for Bioengineering of Catalonia (IBEC), Barcelona Institute of Science and Technology (BIST), Baldiri Reixac 10-12, 08028 Barcelona, Spain

Published online: 02 March 2022

have led to electronic materials and devices with improved mechanical deformability and performance [9, 10]. Within this context, 2D polymeric nanomembranes have attracted much interest because their versatility and excellent features make them very interesting for many bioengineering applications like scaffolds for tissue engineering, drug delivery systems, bioelectronic devices or antimicrobial platforms [11, 12]. The 2D nanomembranes show high macroscopic surface area and nanometric thickness (aspect ratio $> 10^6$) which enables their macroscopic use in a free-standing way as their mechanical integrity/robustness is retain. Moreover, these nanomembranes have high flexibility because, according to the Euler–Bernoulli beam theory, the rigidity of a material, that is the resistance to bending, is proportional to its thickness to the third power [13]. Therefore, flexibility increases as the membrane thickness decreases. These 2D membranes also show excellent conformal contact that can be explained again by their low thickness. Prof. Rogers' group showed that conformability is achieved when thickness is below a critical value where the adhesion energy is larger than the sum of the bending energy of the membrane and the elastic energy of the substrate (e.g., skin). They theoretically demonstrated that the critical value for their elastomeric membranes was ~ 25 µm and they successfully experimentally proved that membranes thinner than this value perfectly conformed onto skin [14]. Apart from those properties, nanomembranes have also attracted great attention due to the possibility to easily tune their architecture from single layered to multilayered nanomembranes and with or without (nano)perforations. Such variability has allowed expanding their applicability range like the transport of metabolites through the nanomembranes, soft actuators, water remediation or biointerfaces as cell matrixes [15–18].

On the other hand, electrically conductive 1D NMs like metal nanowires (NWs) or carbon nanotubes (CNT) have been widely investigated due to characteristics like nanometric size, high aspect ratio and high surface area. Moreover, 1D NMs show unique mechanical deformability due to the high length/diameter ratio making thus brittle metallic materials (e.g., Au, Ag, Cu) interesting for flexible electronics [19]. Moreover, other properties like electrical conductivity are maximized when these NWs are perfectly aligned and non-aggregated. For example, 3D standing NWs have shown higher surface areas and higher conductivity for electrochemical biosensors compared with percolated networks [20, 21]. Other interesting feature of 1D NMs is that they can establish dynamic physicochemical interaction with biological entities like biomolecules, cells or tissues and these interactions can be modulated by tuning NMs properties like surface chemistry, shape, dimension scale and topography. It is therefore crucial to control their surface chemical and physical properties to modulate their interfacial behavior for more efficient performances [22–24]. Usually, NWs have been composited with polymers for bioelectronics applications leading to 3D nanocomposites in which the 1D NWs are randomly distribute. Thus, Hu et al. have prepared a transparent electrode by embedding a percolated network of Cu NWs in polyurethane (PU) [25]. Or Kiran Kumar and coworkers prepared a transparent conductive film based on the dispersion of Ag NWs into hydroxypropyl methyl-cellulose (HPMC) [26].

In this work, a new strategy based on the combination of 2D polymeric nanomembranes hosting vertically aligned cauliflower-like metallic nanowires (NWs) have been designed to overcome the mechanical mismatch of rigid electronics and the low electrical properties of polymeric composites due to aggregation of fillers. Thus, 1D metallic NWs will be grown inside 2D perforated polymeric nanomembranes to develop a functional H_2O_2 biosensor with conformal contact avoiding the mechanical mismatch between tissues and conventional electronics. First, multilayered nanomembranes will be prepared by combining the mechanical properties of poly(lactic acid) (PLA) and the electrochemical behavior of poly(3,4-ethylenedioxythiophene) (PEDOT). While perforated PLA layers will be prepared by spin coating, PEDOT layers will be obtained by electropolymerization. After that, the perforations will host the 1D metallic NWs (e.g., Cu, Cu/Ag) to get well-aligned and highly ordered arrays with improved electrical conductivity to obtain a hybrid 1D NWs-2D nanomembrane as a H_2O_2 sensor with flexibility and conformability. Such strategy is totally different to the most reported works dealing with the fabrication of 3D composites as electrodes in which the 1D NWs are randomly distributed, and mainly aggregated, within a polymeric matrix decreasing their potential advantage [25, 26].

Hydrogen peroxide is a key messenger molecule for cellular signaling and other physiological pathways but its overproduction causes cell oxidative stress resulting in, for example, cardiovascular or neuronal damage [27]. For this reason, the detection of hydrogen peroxide is essential. Among the different methodologies employed (e.g., chemiluminescence) [28], electrochemical methods are preferred due to advantages like fast response, sensitive, economic and easy to use [29]. Enzyme-based electrochemical sensors have been widely studied but they show some drawbacks (e.g., high cost of enzymes, enzyme's activity can be altered depending on pH or temperature, or effective immobilization onto electrode surface is challenging), reason why non-enzymatic sensors are preferred [29]. The non-enzymatic sensors are based on inorganic materials with catalytic properties towards H_2O_2 sensing like carbon nanomaterials, transition metal oxides or noble metals [29]. In this work, we have selected silver due to their catalytic activity to H_2O_2 and their easy deposition onto the electrodeposited Cu nanostructures.

Experimental section

Materials

Aqueous dispersion of poly(3,4-ethylenedioxythiophene):poly(styrene sulfonate) (PEDOT:PSS) (1.3 wt%), 3,4-ethylenedioxythiophene (EDOT) monomer, hydrolyzed poly(vinyl alcohol) (PVA) (87–89%), copper chloride ($CuCl_2$), lithium perchlorate ($LiClO_4$), sodium citrate ($Na_3C_6H_5O_7$), silver nitrate ($AgNO_3$), glucose ($C_6H_{12}O_6$), citric acid ($C_6H_8O_7$) and ascorbic acid ($C_6H_8O_6$) were got from Sigma-Aldrich. $LiClO_4$ was stored in an oven at 80 °C to remove its humidity before use. Poly(lactic acid) pellets (PLA 2002D) were provided by Nupik International. Hydrogen peroxide (H_2O_2) was obtained from Alfa Aesar. Hexafluoroisopropanol (HFIP) and acetonitrile were purchased from Panreac Quimica S.A.U. (Spain).

Methods

Preparation of the nanomembranes and their modification with Cu and Ag

Nanomembranes were prepared by alternatively depositing PLA and PEDOT layers using spin coating and electropolymerization respectively onto a steel substrate (AISI 304) (Area: 3×3 cm^2). First, a PEDOT:PSS sacrificial layer was spin coated (1200 rpm, 60 s) using the 1.3 wt% PEDOT:PSS dispersion. A PLA:PVA layer was subsequently deposited by spin-coating (1200 rpm, 60 s) a mixture of 20 mg mL^{-1} PLA and 20 mg mL^{-1} PVA solutions in HFIP (90:10 v/v PLA:PVA solutions). PVA was selectively etched in water, thus, creating the perforations into the PLA layer. After that, a PEDOT layer was grown by chornoamperomety (Applied potential: 1.4 V vs Ag/AgCl reference electrode, charge: 405 mC) from an acetonitrile solution containing 10 mM EDOT and 0.1 M $LiClO_4$. The subsequent PLA and PEDOT layers were obtained following the previous procedures until obtaining a 5 layered nanomembrane comprising 3 PLA ad 2 PEDOT layers: PLA/PEDOT/PLA/PEDOT/PLA.

Copper 1D nanostructures were grown into the nanomembrane perforations of the top PLA layer by chronopotentiometry using an aqueous solution containing $CuCl_2$ (0.01 M) and sodium citrate (0.1 M). Different intensities in the range from $1 \cdot 10^{-4}$ to $3 \cdot 10^{-3}$ A and variable times (40–800 s) where applied to study their influence on the nanostructure's growth. Following copper nanostructures deposition, Ag was deposited onto Cu nanostructures via a transmetallation reaction. Thus, the Cu-modified nanomembrane was covered with a 20 mM $AgNO_3$ solution for 90 s. After that, the $AgNO_3$ solution was removed and the nanomembrane washed several times with milli-Q water. Finally, the nanomembranes were peel off from the steel substrate by selectively removing the initial sacrificial PEDOT-PSS layer by immersion into milli-Q water for a few hours.

Characterization

Field emission scanning electron microscope (FE-SEM) (Zeiss Model Auriga instrument) was used to observe nanomembrane's morphology. Energy dispersive X-Ray spectroscopy (EDS, Oxford Instrument INCA) attached to the FE-SEM was employed to determine the chemical composition. XPS (X-ray photoelectron spectroscopy) and Auger spectroscopy measurements were performed with a PHI 5600 system and a PHI 670 scanning Auger nanoprobe, respectively. The binding energies (BE) of the XPS peaks were corrected by assuming C1s signal at 284.6 eV. Film thickness was measured by performing eighteen independent measurements in three different samples of each nanomembrane by profilometry (Dektak 150, Veeco). Water sessile drop method was used to evaluate nanomembranes wettability through contact angle measurements (equipment OCA 15EC, Data-Physics Instruments GmbH, Filderstadt). Ten measurements were performed in each sample and images were analyzed by SCA20 software. Fourier transform infrared spectroscopy (FTIR) (Jasco 4100 spectrophotometer) in the wavenumber range 4000–600 cm^{-1} (resolution 4 cm^{-1}) was performed to study the structure of the PLA/PEDOT nanomembranes as well as PLA and PEDOT raw materials. The spectra were an average of 32 scans recorded in each sample.

An AUTOLAB-302N potentiostat/galvanostat was employed to perform the electrochemical experiments. These experiments were made in a conventional three-electrode cell (working electrode: nanomembranes, reference electrode: Ag/AgCl/KCl (3 M), counter electrode: platinum foil) at room temperature. A 0.01 M aqueous phosphate buffered saline (PBS) solution was employed as electrolyte. Cyclic voltammetries (CV) were run in the range 0.0–0.8 V at 200 mV s^{-1}. Electrochemical impedance spectroscopy (EIS) analyses were performed at 10 mV amplitude of the sinusoidal voltage signal in the 10^5–10^{-1} Hz frequency range. An electrical equivalent circuit (EEC) was obtained with the processed EIS results.

Results and discussion

The concept of this research is the combination of two different families of nanomaterials, 2D polymeric nanomembranes and 1D metallic NWs, aiming to incorporate the

best properties of each nanomaterial into a new flexible, conformable and electrically conductive nanostructured ultrathin material as a basis for the development of a biointegrated electrochemical H_2O_2 sensor. The flexible and free-standing 2D polymeric nanomembranes consisted on alternated layers of PLA and PEDOT:PSS. While the PLA layers conferred mechanical stability and contained the nanoperforations to host the nanostructures, PEDOT layers were used for their electrical properties. The PLA/PEDOT multilayered nanomembranes were alternatively deposited using spin coating for PLA layer and electropolymerization for PEDOT one. Figure 1 shows a scheme with the different steps followed to obtain the self-supported PLA/PEDOT nanomembranes. First, a sacrificial PEDOT layer was spin coated onto the steel substrate using the PEDOT:PSS aqueous dispersion (1.3 wt%). This sacrificial layer will be removed by immersing it in water since the non-interacting PEDOT:PSS particles will be redispersed, thus allowing peeling the nanomembrane off the substrate. Second, a nanoperforated PLA layer was obtained by spin coating using a PLA/PVA 90:10 v/v solution following the selective PVA etching in water creating the nanoperforations. After that, chronoamperometry was used to obtain a continuous PEDOT coating onto the previous PLA layer. EDOT monomers were polymerized at a constant potential within the nanoperforations that coalesced after emerging the pores forming the PEDOT layer. Unlike PEDOT sacrificial layer, the PEDOT layer obtained by electropolymerization will remain stable even after immersing in water since it is a continuous and covalently linked layer. Steps 2–4 were repeated to finally obtain nanomembranes with five different layers: PLA/PEDOT/PLA/PEDOT/PLA (5-PLA/PEDOT) (Fig. S1). The top PLA layer was used to host the 1D metallic NWs within the nanometric-size pores, aiming to improve their functionality. Thus, copper was incorporated in the pores using electrodeposition (step 6) since it is a very versatile and easy technique for NMs preparation [30, 31] followed by the formation of a silver layer onto Cu nanostructures through a simple redox reaction (step 7). The incorporation of these 1D NMs is expected to improve the sensibility of the biosensors not only due to the higher electrical conductivity of metals (e.g., Cu, Cu/Ag) but also to the higher surface area of the nanostructures. Moreover, the 1D NWs will be oriented and non-aggregated within the membrane, enhancing even more the surface area and therefore the biosensor response (unlike composites where NMs are randomly oriented and aggregated within the matrix).

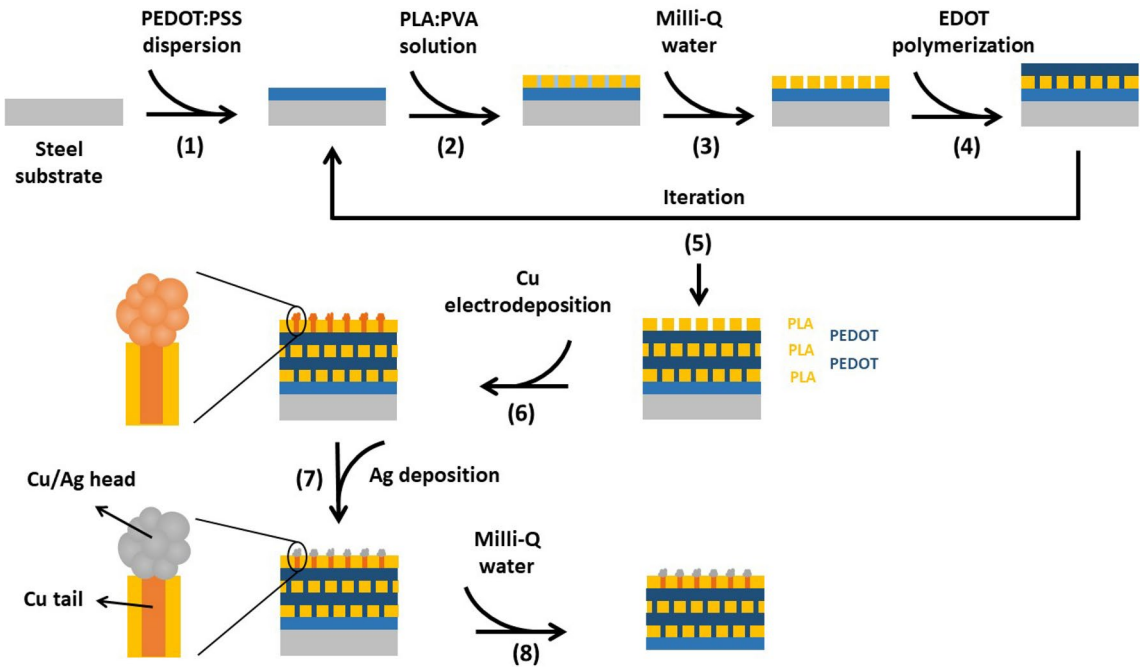

Fig. 1 Schematic illustration showing the fabrication procedure of the 5-PLA/PEDOT, 5-PLA/PEDOT-Cu and 5-PLA/PEDOT-Cu/Ag free-standing nanomembranes. (1) Deposition of the sacrificial PEDOT:PSS layer by spin coating a PEDOT-PSS dispersion. (2) Deposition of a PLA:PVA solution to get a nanosegregated layer. (3) Selective removal of PVA by adding milli-Q water. (4) Growth of a PEDOT layer by EDOT chronoamperometry. (5) The process is repeated until obtaining the PLA/PEDOT/PLA/PEDOT/PLA multilayered nanomembrane (5-PLA/PEDOT). (6) Growth of the 1D cauliflower-shape nanostructures by electrodeposition. (7) Coating Cu nanostructures with a thin Ag layer by a transmetallation reaction. (8) Peeling the membrane off the steel substrate in water to remove the first PEDOT:PSS sacrificial layer

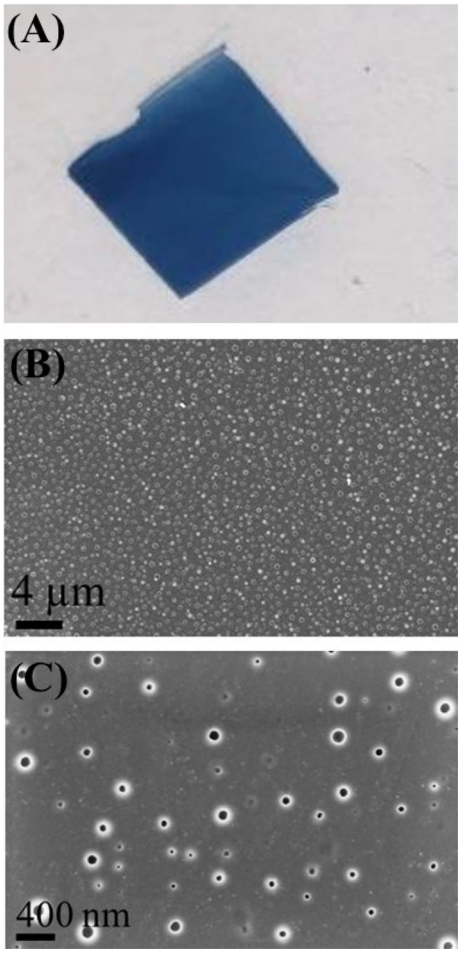

Fig. 2 **A** Optical and **B**, **C** SEM images of the 5-PLA/PEDOT nanomembranes

Figure 2 shows an image of the fabricated 5-PLA/PEDOT nanomembranes as well as SEM micrographs. As it can be observed, the nanomembranes, with the typical blue color of PEDOT, are continuous, homogenous and self-standing. SEM micrographs also show that the membranes are continuous, homogeneous and flat with perforations homogeneously distributed. The perforations are nanometric (76 ± 40 nm) and the estimated pore density is 1.6×10^7 pores cm^{-2}. The thickness of the individual layers and the 5-PLA/PEDOT nanomembrane was studied by profilometry. While the individual PLA and PEDOT layer thicknesses were 158 ± 22 nm and 178 ± 24 nm, respectively, the 5-PLA/PEDOT nanomembrane was 731 ± 32 nm thick. The total thickness is lower than the arithmetic sum of the individual layers because of the compression of the lower layers due to the upper ones. On the other hand, the FTIR analysis of the 5-PLA/PEDOT nanomembranes reveal the presence of the main peaks of PLA [1750 cm^{-1} (C=O) stretching vibration, 1180 cm^{-1} asymmetric C–O stretching, 1085 cm^{-1} symmetric C–O stretching] and PEDOT (1527 cm^{-1} C=C stretching, 1230 and 1040 cm^{-1} C–O–C stretching, 845 cm^{-1} C–S stretching) but a bit shifted with respect their positions in the raw PLA and PEDOT:PSS. This shift is indicative of some weak Van der Waals interactions at the interface between the PLA and PEDOT layers (Fig. S2).

After that, the 5-PLA/PEDOT nanomembranes were modified with the metallic NMs to improve their functionality. First, Cu NWs were first grown by electrodeposition into the perforations aiming to improve electrical conductivity of the nanomembrane. And second, Ag was coated onto previous Cu nanostructures by a transmetallation reaction. Silver confers electrocatalytic properties towards H_2O_2, biocompatibility and corrosion resistance as well as high faradaic current density, fast electron transfer rate and high signal-to-noise ratio while keeping the high electrical conductivity [32, 33]. Herein, the nanomembranes are denoted 5-PLA/PEDOT-Cu and 5-PLA/PEDOT-Cu/Ag, respectively. Electrodeposition of Cu was performed by chronopotentiometry at different conditions of current density and time (Figure S3). The SEM analysis revealed that at low current densities no growth of Cu outside the membrane was observed. However, for an applied current density of − 1.4 mA cm^{-2} during 40 s, we obtained nanostructures with a cauliflower-shape morphology with nanoparticles (NPs) as the "head" and NWs as the "tail". Such nanostructures result from the complete filling of the pores and moderate growth outside them (Fig. 3A, B). For higher times or current densities,

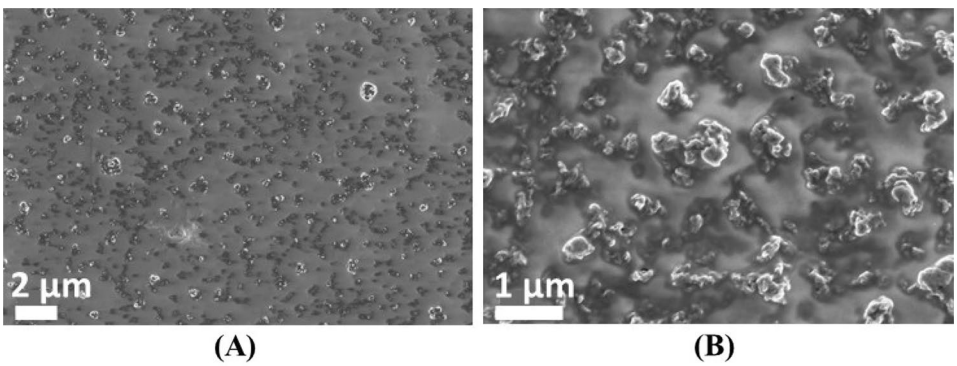

Fig. 3 **A**, **B** SEM images of the 5-PLA/PEDOT-Cu nanomembranes after copper electrodeposition at − 1.4 mA cm^{-2} during 40 s at different magnifications

these nanostructures grew in size and even coalesced leading to a continuous layer (Figure S4). These conditions are avoided since a nanostructured surface is preferred over a continuous coating to maximize surface area and, therefore, have a higher response towards H_2O_2. The presence of Cu is clearly detected by EDX spectroscopy (Fig. 4A). Other elements (e.g., Fe, Ni, Cr) were also detected coming from the AISI 304 steel substrate used to prepare the nanomembranes. Finally, Ag was coated onto the Cu nanostructures by covering the 5-PLA/PEDOT-Cu nanomembrane's surface with a 20 mM $AgNO_3$ solution for 90 s. During this time, the transmetallation reaction between metallic Cu and Ag^+ ions took place leading to an Ag metallic coating onto the Cu nanostructures ($Cu + 2Ag^+ \rightarrow Cu^{2+} + 2Ag$). As we observed by SEM, the presence of the Ag layer did not modify the cauliflower shape of Cu that was probably attributed to the nanometric thickness of the silver layer. XPS analysis confirmed the presence of Ag layer (Fig. 4B). XPS spectrum shows two peaks at binding energies (BE) of 367 and 373 nm attributed to the spin–orbit components $3d_{5/2}$ and $3d_{3/2}$ of Ag, respectively. On the other hand, a calculated full width half maximum (FWHM) of 1.4 eV is in accordance with the reported values for metallic Ag (FWHM = 1.2 eV). Moreover, the following characteristics also corresponds to Ag^0: (1) the energy distance (ΔBE) between the two peaks is 6.0 eV, (2) the peaks are asymmetric and (3) the presence of loss features observed at the higher BE side of each peak [34, 35].

The membranes were easily peel off from the steel substrate by dipping them in water due to the easy redispersion of the initial PEDOT:PSS sacrificial layer. The free nanomembranes are (1) self-supportive as they keep intact after releasing them from the substrate; (2) flexible/foldable, and (3) conformable on many surfaces. Nanomembrane's robustness and flexibility can be observed since they can be picked up by a pipette, stored and released without damaging (Videos S1). Moreover, according to the Euler–Bernoulli theory, flexibility is dependent on the inverse of thickness to the third power, meaning that materials are more prone to bent when thickness decreases [13]. In this sense, we have checked that the fabricated nanomembranes can be bent 180° for a high number of times (> 100) without experience any damage confirming their high flexibility. The bending capacity of the membranes is also observed as they completely adapt onto a curved pipette tip (Video S2) with a bending angle of 180°. Regarding conformability, nanomembranes completely adapt to substrates with different shapes faithfully reproducing their surfaces like a rigid glass slide (planar, rigid substrate), a flexible polyethylene terephthalate (PET) film (planar, flexible substrate), a plastic pipette tip (flexible, rounded substrate), a lemon or a hairy kiwi (curvilinear, rough substrates) or a dynamic finger (curvilinear, rough substrate) (Figure S5, Videos S1–S3). Again, such conformal contact was attributed to the low membrane thickness [14]. It is also worthy to mention that the nanomembranes were totally stable onto those surfaces for long periods of times without experiencing any damage. Finally, the nanomembranes recovered their planarity after immersing them back in water. Although this means that they do not adhere onto wet surfaces, this is not a drawback since the main applications of the membranes will be onto non-wetted surfaces (e.g., adapted onto skin). A future work would be making these membranes adhesive even onto wet substrates by adding, for example, polydopamine during membrane fabrication.

With these Cu/Ag-modified nanomembranes, we developed a non-enzymatic electrochemical H_2O_2 biosensor based on the catalytic properties of Ag towards this molecule. The development of easy, fast, flexible and conformable sensors for H_2O_2 is increasing because this molecule has a key role in many fields (e.g., textile, environmental, food, pharmaceutical) but especially for health monitoring due to its participation in many biological processes like diabetes, cancer, neurodegeneration or aging [36]. Although great progress has been made in recent years, so far most of the reported H_2O_2 electrochemical sensors are in rigid form, which limits

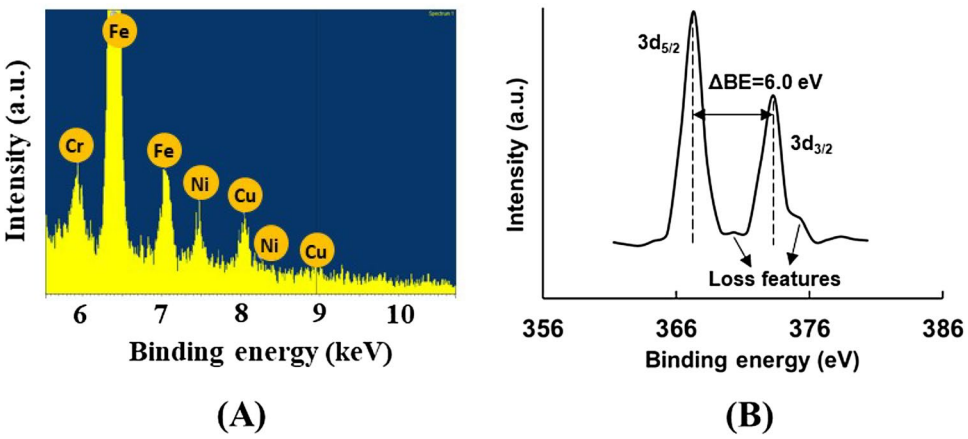

Fig. 4 **A** EDX spectrum of the 5-PLA/PEDOT-Cu nanomembrane. **B** XPS spectrum of the 5-PLA/PEDOT-Cu/Ag nanomembrane

their wide application in wearable electronics. First, the electrochemical performance of the modified (5-PLA/PEDOT-Cu, 5-PLA/PEDOT-Cu/Ag) and non-modified (5-PLA/PEDOT) nanomembranes was assessed by cyclic voltammetry in the absence of H_2O_2 (Fig. 5A). The current density increases in the following order 5-PLA/PEDOT < 5-PLA/PEDOT-Cu < 5-PLA/PEDOT-Cu/Ag due to the good electrical conductivity of Cu ($\sigma = 5.96 \cdot 10^7$ S m^{-1}) and the better electrical conductivity of Ag ($\sigma = 6.30 \cdot 10^7$ S m^{-1}). Later, EIS analyses were conducted on the same samples to assess the influence of Cu and Ag on the electrochemical properties of the nanomembranes. The ion transport was evaluated by measuring the impedance for frequencies ranging from 10^5 to 10^{-1} Hz in a 0.5 M NaCl solution. Nyquist plots shows the imaginary impedance, indicative of the capacitive/inductive behaviour, against the real impedance ($-Z''$ vs Z') (Fig. 5B). In a Nyquist plot, the semi-circular response is attributed to the electron transfer resistance at the higher frequency values (bulk resistance, R_p), which determines the electron transfer kinetics of the redox probe at the electrode–electrolyte interface. The incorporation of Cu nanostructures has substantially changed the electrochemical response of the nanomembrane compared to the bare one. As can be observed, a semicircle with a large diameter is only observed for 5-PLA/PEDOT, which is associated with a very large R_p (90.5 MΩ) assuming a simplified Randles-like equivalent circuit (Figure S6) in which a CPE (constant phase element) element is used. Meanwhile, the 5-PLA/PEDOT-Cu sample exhibits a semicircle with a much smaller diameter that accounts for a lower R_p (683 kΩ) upon adjustment to a Randles-like circuit (Figure S6) indicating the successful incorporation of Cu into the membrane nanoperforations. In the same line, the EIS spectrum of 5-PLA/PEDOT-Cu/Ag nanomembrane shows a semicircle with an even smaller diameter than 5-PLA/PEDOT-Cu leading to the lowest R_p (39.7 kΩ), assuming a Randles-like circuit (Figure S6), among the different nanomembranes. These results are in accordance with the CV and clearly show the improvement in the electrical conductivity of the nanomembranes after Cu incorporation and even higher conductivity after its coating with Ag. Figure 5C shows a magnification of the left part of the Nyquist plot in Fig. 5B. The pseudo-capacitive behaviour that is noticed in the samples through the presence of the capacitive spike is mainly attributed to the PEDOT/PLA layers. The decreasing slope of the capacitive tail for the 5-PLA/PEDOT-Cu and even more for the 5-PLA/

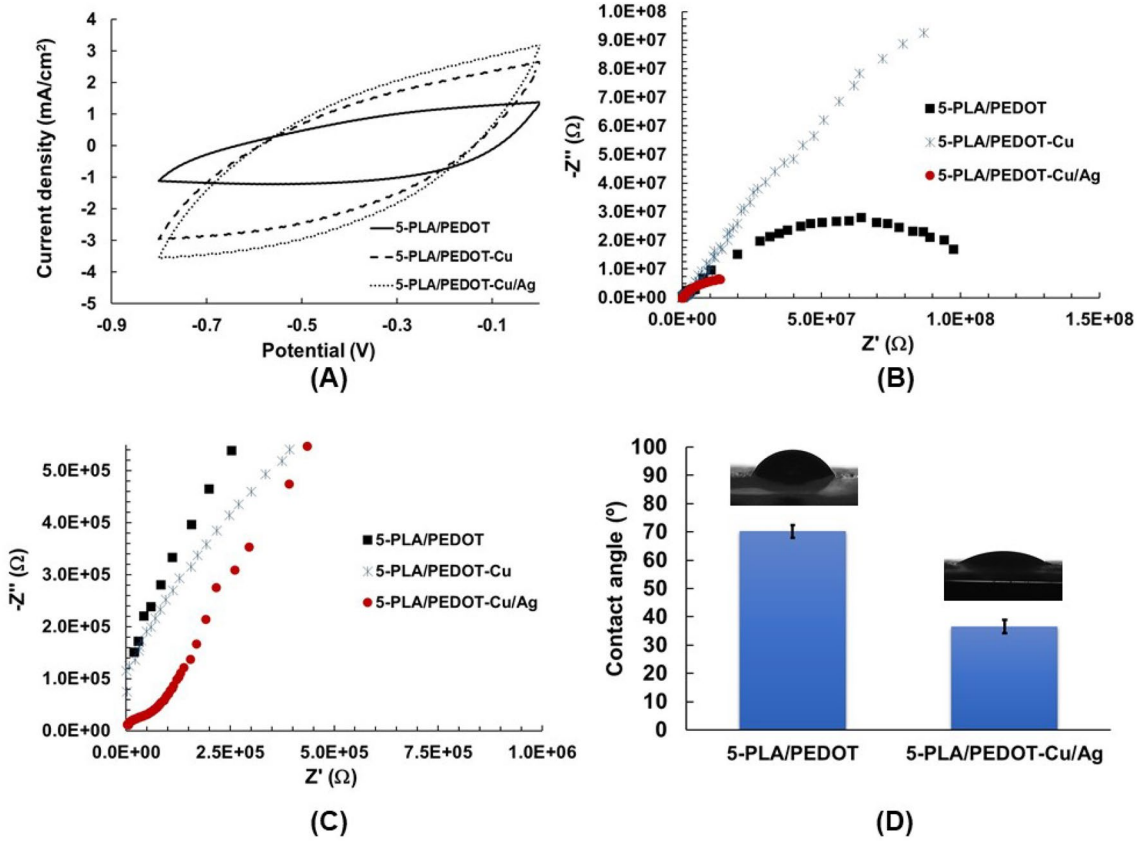

Fig. 5 **A** Cyclic voltammetries, **B** Niquist plots and **C** magnified Niquist plots for the 5-PLA/PEDOT, 5-PLA/PEDOT-Cu and 5-PLA/PEDOT-Cu/Ag nanomembranes. **D** Water contact angle of 5-PLA/PEDOT and 5-PLA/PEDOT-Cu/Ag nanomembranes

PEDOT-Cu/Ag is due to the presence of Cu or Cu/Ag metals, confirming again a nanomembrane resistance drop.

The contact angles (θ) measured in water (Fig. 5D) also provided indirect evidence of the successful modification of 5-PLA/PEDOT with the metallic nanostructures. The wettability of 5-PLA/PEDOT significantly increased upon the incorporation of Cu/Ag as the water contact angle decreased from $70.1° \pm 2.9°$ for 5-PLA/PEDOT to $36.5° \pm 2.3°$ for 5-PLA/PEDOT-Cu/Ag. The increased wettability is due to the metallic nanostructures, characterized by high surface energy which favors hydrophilic behavior and lead water droplets to immediately spread on the surface [37].

Based on previous results and since the 5-PLA/PEDOT-Cu/Ag nanomembrane showed better properties (e.g., higher current density, lower charge transfer resistance and higher wettability) than the other samples, we evaluated its performance as electrode for H_2O_2 sensing. Different H_2O_2 concentrations were added to build the calibration plot and determine the sensitivity as well as the limit of detection (LOD) of the electrochemical sensor. Figure 6A shows the CVs recorded in different solutions containing H_2O_2 concentrations in the range 0.35–10 mM. As it can be observed, the current density at negative potentials increases after each addition due to the catalytic reduction of H_2O_2 due to the presence of silver. From the previous data, the current density-H_2O_2 concentration calibration plot was obtained showing a linear dependence between the current density and the concentration up to 10 mM (Fig. 6B). In this range, the precision is very high, as reflected in the R-squared value provided by the linear fit ($R^2 = 0.9971$). A good sensitivity of 120.3 ± 8.6 µA cm^{-2} mM^{-1} was obtained from the absolute value of the slope of the calibration line and a low LOD (7.0 ± 0.4 µM) was calculated as the ratio between three times the standard deviation of the blank solution (without addition H_2O_2) and the absolute value of the slope of the calibration curve [38]. The low standard deviations for the sensitivity and LOD indicate the good repeatability of the nanomembranes for H_2O_2 sensing. Table 1 shows a comparison of the performance of the nanomembrane developed in this work with other similar flexible non-enzymatic H_2O_2 sensors in the literature (Table 1). Similar sensitivity, linear range and LOD can be observed when compared with reported sensors based only on Ag NMs like our study. For example, Lee et al. developed Ag NW-based films by vacuum filtration. The films, formed by a homogenous and non-oriented Ag NWs network, displayed a LOD of 46 µM [39]. Hsiao et al. prepared urchin-like Ag NWs based electrodes by screen printing showing a detection limit of 10 µM [40]. Or Kurowska and coworkers fabricated an AgNW array by electrodeposition using an aluminum oxide (AAO) as template to grow the silver nanostructures. After AAO removal, the array showed

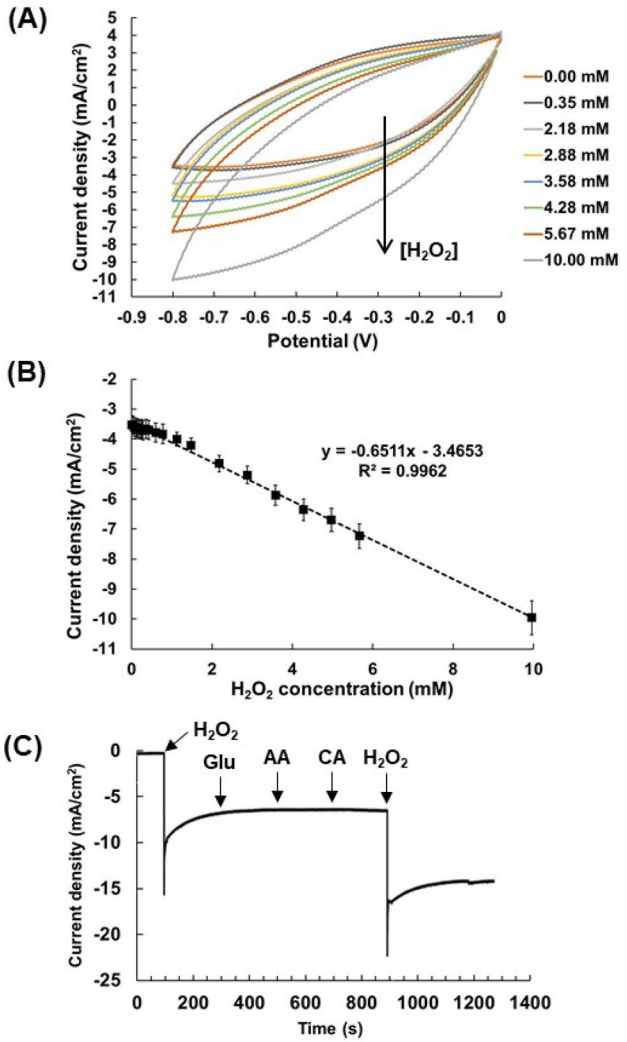

Fig. 6 **A** Cyclic voltammetries recorded at different H_2O_2 concentrations (from 0 to 10 mM) using 5-PLA/PEDOT-Cu/Ag nanomembrane as working electrode. Scan rate: 200 mV s^{-1}. **B** Calibration plot obtained from graph (**A**). **C** Chronoamperometry curve to evaluate the interference properties of the 5-PLA/PEDOT-Cu/Ag by adding glucose, ascorbic acid and citric acid

a LOD of 29.2 µM [41]. Thus, the LOD of our 5-PLA/PEDOT-Cu/Ag nanomembranes is much better than the previously reported Ag NWs-based sensors which we attribute either to the random orientation of the NWs [39, 40] or some agglomeration after template removal [41]. If we compare with Ag-based composite systems (e.g., Graphene/Ag NPs) [42, 43] or with other materials (e.g., MnO_2, $PtTe_2$) [29, 44–46], the LOD value found in this work is similar or slightly higher than those. For example, the work of Aparicio-Martinez and coauthors showed a LOD of 7.9 µM for a graphene electrode decorated with Ag NPs using laser irradiation [42]. Or Gholami and Koivisto quantified a LOD of 0.48 µM for carbon fibers coated with Ag NPs and embedded into nafion [43]. Lower

Table 1 Performance of different non-enzymatic H_2O_2 sensors found in the literature

Electrode materials	Sensitivity	Linear range (mM)	LOD (mM)	References
Ag NWs/PET	749 μA mM^{-1} cm^{-2}	0.2–1.5	46	[39]
		1.7–3.4		
Ag NWs/carbon electrode	4705 μA mM^{-1} mg^{-1} cm^{-2}	0.05–10.35	10	[40]
Ag NWs array/Cu	26.6 μA mM^{-1} cm^{-2}	0.1–3.1	29.2	[41]
Ag NPs/graphene	32 μA mM^{-1}	0.1–10	7.9	[42]
Ag NPs/carbon microfibres/nafion	–-	0.1–80	0.48	[43]
Ag/MnO_2/MWCNT/GCE	82.5 μA mM^{-1} cm^{-2}	0.005–10.4	1.7	[44]
MnO_2/graphite nanofibres	1096 μA mM^{-1} cm^{-2}	0.1–11	1.25	[45]
MnO_2/graphene nanosheets/GCE	422.1 μA mM^{-1} cm^{-2}	0.0005–3.5	0.19	[29]
$PtTe_2$/GCE	10.9 μA mM^{-1}	0.003–0.3	1.2	[46]
		0.5–1.1		

NPs nanoparticles, *MWCNT* multiwalled carbon nanotube, *GCE* glassy carbon electrode

LODs have been achieved with electrodes based on MnO_2 (e.g., MnO_2/Graphene nanosheets) (LOD = 0.19 μM) [29] or $PtTe_2$ (LOD = 1.2 μM) [46].

Nowadays, there is a controversy about the normal H_2O_2 levels found in body fluids for healthy people. While some studies report that those levels in plasma should be around 10 μM, other works report values higher than 20 μM [47]. Regarding other body fluids, concentrations of hydrogen peroxide of 100 μM or higher have been founded in freshly voided human urine and vitreous humor of healthy persons [48]. However, what it seems clear is that H_2O_2 concentrations higher than 20 mM triggers inflammatory responses and values higher than 50 μM are cytotoxic to a wide range of cultured animal, plant and bacterial cells [48]. Moreover, it has been found that levels in the range 30–50 μM are present in certain diseases or during chronic inflammation [47]. Despite the disparity of values, we believe that the LOD reported in this work for the fabricated nanomembranes allows detecting H_2O_2 concentrations for healthy and sick people. At this point, we would like to comment that different strategies could be followed to improve the LOD of the nanomembranes like (1) increasing the surface area by increasing pore density in the membrane, reducing pore size or conferring mesoporosity to the Cu nanostructures during electrodeposition, and (2) decorating Cu/Ag nanostructures with transition metal oxides or dichalcogenides as they seem having a better response towards H_2O_2.

Finally, the stability and interference properties of the 5-PLA/PEDOT-Cu/Ag nanomembranes were evaluated. CV was employed to quantify the stability of the samples 2 months after their preparation; a 5 mM H_2O_2 solution showed a 95.5 ± 1.3% retention of the initial current density. The good stability results can be attributed to the noble character of silver as a sensing material. Finally, the anti-interference experiments were performed by chronoamperometry (Fig. 6C). No significant current changes were observed after adding some common interfering substances like glucose (Glu), ascorbic acid (AA) or citric acid (CA) indicating the good selectivity of the nanomembranes towards H_2O_2. Thus, we have demonstrated that 5-PLA/PEDOT-Cu/Ag nanomembranes can be successfully used as electrodes with flexibility and conformability over different substrates with good electrochemical performance (e.g., sensitivity, LOD, linear range) as well as good stability, reproducibility, and selectivity for H_2O_2 sensing.

Conclusions

In summary, 1D metallic and 2D polymeric nanoblocks have been successfully combined to obtain free-standing hydrid nanomembranes with flexibility and conformability over many and varied surfaces. The PLA/PEDOT nanomembranes have been fabricated by alternatively using spin coating and chronoamperometry. Cauliflower-shape 1D Cu nanostructures have been successfully electrodeposited onto the perforations of the top PLA layer as observed by SEM and EDX. Silver was subsequently coated onto Cu by a transmetallation reaction as detected by XPS. The 5-PLA/PEDOT-Cu/Ag nanomembranes showed the highest current density, the lowest charge transfer resistance and highest wettability due to the Cu/Ag nanostructures present in the nanomembrane. These nanomembranes were successfully employed as electrodes for H_2O_2 sensing showing good linear concentration range (0.35–10 mM), sensitivity (120 μA cm^{-2} mM^{-1}) and LOD (7 μm) as well as good reproducibility, stability and selectivity.

Supplementary Information The online version contains supplementary material available at https://doi.org/10.1007/s40097-022-00482-5.

Acknowledgements Authors acknowledge MINECO-FEDER (RTI2018-098951-B-I00 and PID2019-103892RB-I00/AEI/10.13039/501100011033) and Agència de Gestió d'Ajuts Universitaris i de Recerca de Catalunya (2017SGR359 and 2017SGR-1165) for financial support. M.-P.G. and C.A. received support for the research from the Generalitat de Catalunya through the prize "ICREA Academia". J.G.-T. acknowledge the Serra Hunter program of the Generalitat de Catalunya.

Author contributions JG-T: conceptualization; formal analysis; resources; supervision; validation; visualization; writing—original draft; writing—review and editing. CL: investigation. DS: investigation; writing—review and editing. SL: investigation; formal analysis. M-PG: funding acquisition, project administration, writing—review and editing. CA: conceptualization; formal analysis; resources; supervision; validation; funding acquisition; project administration; writing—review and editing.

Funding Open Access funding provided thanks to the CRUE-CSIC agreement with Springer Nature.

Declarations

Conflict of interest The authors declare no competing interests.

References

1. Vazquez-Guardado, A., Yang, Y., Bandodkar, A.J., Rogers, J.A.: Recent advances in neurotechnologies with broad potential for neuroscience research. Nat. Neurosci. **23**, 1522–1536 (2020)
2. Yeo, W.H., Kim, Y.S., Lee, J., Ameen, A., Shi, L., Li, M., Wang, S., Ma, R., Jin, S.H., Kang, Z., Huang, Y., Rogers, J.A.: Multifunctional epidermal electronics printed directly onto the skin. Adv. Mater. **25**, 2773–2778 (2013)
3. Wang, L., Jiang, K., Shen, G.: Wearable, implantable, and interventional medical devices based on smart electronic skins. Adv. Mater. Technol. **6**, 2100107:1-2100107:18 (2021)
4. Rich, S.I., Jiang, Z., Fukuda, K., Someya, T.: Well-rounded devices: the fabrication of electronics on curved surfaces—a review. Mater. Horizons **8**, 1926–1958 (2021)
5. Liu, J., Yan, D., Pang, W., Zhang, Y.: Design, fabrication and applications of soft network materials. Mater. Today **49**, 324–350 (2021)
6. Lee, W., Yun, H., Song, J.-K., Sunwoo, S.-H., Kim, D.-H.: Nanoscale materials and deformable device designs for bioinspired and biointegrated electronics. Acc. Mater. Res. **2**(4), 266–281 (2021)
7. Wagner, S., Bauer, S.: Materials for stretchable electronics. MRS Bull. **37**, 207–213 (2012)
8. Shin, M.K., Oh, J., Lima, M., Kozlov, M.E., Kim, S.J., Baughman, R.H.: Elastomeric conductive composites based on carbon nanotube forests. Adv. Mater. **22**(24), 2663–2667 (2010)
9. Lee, J., Yang, J., Kwon, S.G., Hyeon, T.: Nonclassical nucleation and growth of inorganic nanoparticles. Nat. Rev. Mater. **1**, 16034 (2016)
10. Yang, J., Choi, M.K., Kim, D.-H., Hyeon, T.: Designed assembly and integration of colloidal nanocrystals for device applications. Adv. Mater. **28**, 1176–1207 (2016)
11. Puiggalí-Jou, A., Medina, J., del Valle, L.J., Alemán, C.: Nanoperforations in poly(lactic acid) free-standing nanomembranes to promote interactions with cell filopodia. Eur. Polym. J. **75**, 552–564 (2016)
12. Puiggalí-Jou, A., Pérez-Madrigal, M.M., del Valle, L.J., Armelin, E., Casas, M.T., Michaux, C., Perpète, E.A., Estrany, F., Alemán, C.: Confinement of a β-barrel protein in nanoperforated free-standing nanomembranes for ion transport. Nanoscale **8**, 16922–16935 (2016)
13. Liu, Y., Pharr, M., Salvatore, G.A.: Lab-on-skin: a review of flexible and stretchable electronics for wearable health monitoring. ACS Nano **11**, 9614–9635 (2017)
14. Jeong, J.-W., Yeo, W.-H., Akhtar, A., Norton, J.J.S., Kwack, Y.-J., Li, S., Jung, S.-Y., Su, Y., Lee, W., Xia, J., Cheng, H., Huang, Y., Choi, W.-S., Bretl, T., Rogers, J.A.: Materials and optimized designs for human–machine interfaces via epidermal electronics. Adv. Mater. **25**, 6839–6846 (2013)
15. Son, D., Lee, J., Qiao, S., Ghaffari, R., Kim, J., Lee, J.E., Song, C., Kim, S.J., Lee, D.J., Jun, S.W., Yang, S., Park, M., Shin, J., Do, K., Lee, M., Kang, K., Hwang, C.S., Lu, N.S., Hyeon, T., Kim, D.H.: Multifunctional wearable devices for diagnosis and therapy of movement disorders. Nat. Nanotechnol. **9**, 397–404 (2014)
16. Molina, B.G., Cuesta, S., Besharatloo, H., Roa, J.J., Armelin, E., Aleman, C.: Free-standing faradaic motors based on biocompatible nanoperforated poly(lactic acid) layers and electropolymerized poly(3,4-ethylenedioxythiophene). ACS Appl. Mater. Interf. **11**, 29427–29435 (2019)
17. Molina, B.G., Lopes-Rodrigues, M., Estrany, F., Michaux, C., Perpète, E.A., Armelin, E., Aleman, C.: Free-standing flexible and biomimetic hybrid membranes for ions and ATP transport. J. Membr. Sci. **601**, 117931 (2020)
18. Puri, N., Gupta, A., Mishra, A.: Recent advances on nano-adsorbents and nanomembranes for the remediation of water. J. Clean. Prod. **322**, 129051 (2021)
19. Gong, S., Cheng, W.: One-dimensional nanomaterials for soft electronics. Adv. Electron. Mater. **3**(3), 1600314 (2017)
20. Wang, Y., Gong, S., Gomez, D., Ling, Y., Yap, L.W., Simon, G.P., Cheng, W.: Unconventional Janus properties of enokitake-like gold nanowire films. ACS Nano **12**, 8717–8722 (2018)
21. Gong, S., Wang, Y., Yap, L.W., Ling, Y., Zhao, Y., Dong, D., Shi, Q., Liu, Y., Uddin, H., Cheng, W.: A location- and sharpness-specific tactile electronic skin based on staircase-like nanowire patches. Nanoscale Horizons **3**, 640–647 (2018)
22. Tonga, G.Y., Saha, K., Rotello, V.M.: 25th Anniversary article: Interfacing nanoparticles and biology: new strategies for biomedicine. Adv. Mater. **26**, 359–370 (2014)
23. Cho, K.W., Sunwoo, S.-H., Hong, Y.J., Koo, J.H., Kim, J.H., Baik, S., Hyeon, T., Kim, D.-H.: Soft bioelectronics based on nanomaterials. Chem. Rev. (2021). https://doi.org/10.1021/acs.chemrev.1c00531
24. Shi, Y., Liu, K., Zhang, Z., Tao, X., Chen, H.-Y., Kingshott, P., Wang, P.-Y.: Decoration of material surfaces with complex physicochemical signals for biointerface applications. ACS Biomater. Sci. Eng. **6**(4), 1836–1851 (2020)

25. Hu, W., Wang, R., Lu, Y., Pei, Q.: An elastomeric transparent composite electrode based on copper nanowires and polyurethane. J. Mater. Chem. C **2**, 1298–1305 (2014)
26. Kiran Kumar, A.B.V., Wan Bae, C., Piao, L., Kim, S.-H.: Silver nanowire based flexible electrodes with improved properties: high conductivity, transparency, adhesion and low haze. Mater. Res. Bull. **48**, 2944–2949 (2013)
27. Giorgio, M., Trinei, M., Migliaccio, E., Pelicci, P.G.: Hydrogen peroxide: a metabolic by-product or a common mediator of ageing signals? Nat. Rev. Mol. Cell Biol. **8**, 722–728 (2007)
28. Jones, M.R., Lee, K.: Determination of environmentally H_2O_2 for extended periods by chemiluminsecence with real-time inhibition of iron interferences. Microchem. J. **147**, 1021–1027 (2019)
29. Guan, J.F., Huang, Z.N., Zou, J., Jiang, X.Y., Peng, D.M., Yu, J.G.: A sensitive non-enzymatic electrochemical sensor based on acicular manganese dioxide modified graphene nanosheets composite for hydrogen peroxide detection. Ecotoxicol. Environ. Saf. **190**, 110123 (2020)
30. Serrà, A., García-Torres, J.: Electrochemistry: a basic and powerful tool for micro- and nanomotor fabrication and characterization. Appl. Mater. Today **22**, 100939:1-100939:23 (2021)
31. Garcia-Torres, J., Gomez, E., Valles, E.: Measurement of the giant magnetoresistance effect in cobalt-silver magnetic nanostructures: nanowires. J. Phys. Chem. C **116**(22), 12250–12257 (2012)
32. Zhao, Q., Zhao, M., Qiu, J., Lai, W.-Y., Pang, H., Huang, W.: One dimensional silver-based nanomaterials: preparations and electrochemical applications. Small **13**(38), 1701091:1-1701091:18 (2017)
33. Brzózka, A., Brudzisz, A., Jeleń, A., Kozak, M., Wesół, J., Iwaniec, M., Sulka, G.D.: A comparative study of electrocatalytic reduction of hydrogen peroxide at carbon rod electrodes decorated with silver particles. Mater. Sci. Eng. B **263**, 114801:1-114801:12 (2021)
34. Carapeto, A.P., Ferraria, A.M., do Rego, A.M.B.: Silver nanoparticles on cellulose surfaces: quantitative measurements. Nanomaterials **9**, 7801–7808 (2019)
35. Garcia-Torres, J., Valles, E., Gomez, E.: Synthesis and characterization of Co@Ag core–shell nanoparticles. J. Nanopart. Res. **12**, 2189–2199 (2010)
36. Chen, W., Cai, S., Ren, Q.-Q., Wen, W., Zhao, Y.-D.: Recent advances in electrochemical sensing for hydrogen peroxide: a review. Analyst **137**, 49–58 (2012)
37. Taleb, A., Mangeney, C., Ivanova, V.: Electrochemical synthesis using a self-assembled Au nanoparticle template of dendritic films with unusual wetting properties. Nanotechnology **22**, 205301 (2011)
38. Forootan, A., Sjöback, R., Björkman, J., Sjögreen, B., Linz, L., Kubista, M.: Methods to determine limit of detection and limit of quantification in quantitative real-time PCR (qPCR). Biomol. Detect. Quantif. **12**, 1–6 (2017)
39. Lee, J.H., Huynh-Nguyen, B.-C., Ko, E., Kim, J.H., Seong, G.H.: Fabrication of flexible, transparent silver nanowire electrodes foramperometric detection of hydrogen peroxide. Sens. Actuators B **224**, 789–797 (2016)
40. Hsiao, W.H., Chen, H.Y., Cheng, T.M., Huang, T.K., Chen, Y.L., Lee, C.Y., Chiu, H.T.: Urchin-like Ag nanowires as non-enzymatic hydrogen peroxide sensor. J. Chin. Chem. Soc. **59**, 500–506 (2012)
41. Kurowska, E., Brzozka, A., Jarosz, M., Sulka, G.D., Jaskuła, M.: Silver nanowire array sensor for sensitive and rapid detection of H_2O_2. Electrochim. Acta **104**, 439–447 (2013)
42. Aparicio-Martínez, E., Ibarra, A., Estrada-Moreno, I.A., Osuna, V., Dominguez, R.B.: Flexible electrochemical sensor based on laser scribed Graphene/Ag nanoparticles for non-enzymatic hydrogen peroxide detection. Sens. Actuators B **301**, 127101–127108 (2019)
43. Gholami, M., Koivisto, B.: A flexible and highly selective non-enzymatic H_2O_2 sensor based on silver nanoparticles embedded into Nafion. Appl. Surf. Sci. **467–468**, 112–118 (2019)
44. Han, Y., Zheng, J., Dong, S.: A novel nonenzymatic hydrogen peroxide sensor based on Ag–MnO_2–MWCNTs nanocomposites. Electrochim. Acta **90**, 35–43 (2013)
45. Ramachandran, K., Zahoor, A., Kumar, T.R., Nahm, K.S., Balasubramani, A., Kumar, G.G.: MnO_2 nanorods grown NGNF nanocomposites for the application of highly sensitive and selective electrochemical detection of hydrogen peroxide. J. Ind. Eng. Chem. **46**, 19–27 (2017)
46. Rohaizad, N., Mayorga-Martinez, C.C., Sofer, Z., Webster, R.D., Pumera, M.: Layered platinum dichalcogenides (PtS_2, $PtSe_2$, $PtTe_2$) for non-enzymatic electrochemical sensor. Appl. Mater. Today **19**, 100606 (2020)
47. Forman, H.J., Bernardo, A., Davies, K.J.A.: What is the concentration of hydrogen peroxide in blood and plasma? Arch. Biochem. Biophys. **603**, 48–53 (2016)
48. Halliwell, B., Clement, M.V., Long, L.H.: Hydrogen peroxide in the human body. FEBS Lett. **486**, 10–13 (2000)